Selective monostability in multi-stable systems

R. Sevilla-Escoboza, A. N. Pisarchik, R. Jaimes-Reátegui, and G. Huerta-Cuellar

We propose a robust method which allows to transform a periodic or a chaotic multi-stable system to a monostable system at an orbit with dominant frequency of any of the coexisting attractors. Our approach implies the selection of a particular attractor by periodic external modulation with frequency close to the dominant frequency in the power spectrum of a desired orbit and simultaneous annihilation of all other coexisting states by positive feedback, both applied to one of the system parameters. The method does not require a preliminary knowledge of the system dynamics and the phase space structure. The efficiency of the method is demonstrated in both a non-autonomous multistable laser with coexisting periodic orbits and an autonomous Rössler-like oscillator with coexisting chaotic attractors. The experiments with an erbium-doped fiber laser provide evidence for the robustness of the proposed method in making the system monostable at an orbit with dominant frequency of any preselected attractor.

Multistability is a universal, essentially nonlinear phenomenon that has been found in almost all areas of science and nature – from lasers [1, 2] and chemical reactions [3] to climate [4, 5] and brain [6, 7]. Multistability also contributes to fundamental dynamics of neurons and neuronal networks [8–10] involving cell differentiation and hysteresis and is compulsory for implementing associative memories, signal processing, pattern recognition, and optimization problems [11–13]. The coexistence of attractors often appears in systems with time-delayed feedback [14, 15] and in systems with small dissipation [4].

In a real system with multiple coexisting attractors, it is very difficult to keep the trajectory in a particular attractor due to extremely high sensitivity of the multistable system to external perturbations or noise. Several feedback and non-feedback control strategies have been developed to direct the system trajectory to a desired attractor (see [4] and references therein). Feedback control [16–19] and forecast-based control [20] methods allow attractor selection without changing the structure of basins of attraction. Instead, non-feedback control, e.g. in the form of external modulation [21–23], destroys some of attractors resulting in monostability, but it does not allow in every case to select a particular attractor. In practice, the possibility to convert a multistable system to a monostable one is very much in demand because this would allow one to avoid any unpredictable switch to another coexisting state that may be caused by environmental fluctuations or increasing internal noise. Modern engineering and laser technologies require not only a stable output, robust to noise and sudden surges in parameters or variables [24–27], but also the possibility to choose a state with specific properties. Multistability has to be avoided not only in engineering, but also in medicine, where serious diseases such as epilepsy [7, 28] and cardiac arrhythmia [29, 30] is thought to be caused by the coexistence of normal and pathological states.

Although the transformation from multistable to monostable regime can be often achieved by just changing parameter values, in many situations a large variation of system parameters is undesirable and even not always possible. As we already mentioned above, due to several limitations, the existing methods for controlling multistability are not able to make a system monostable at an attractor with characteristic properties of any one of coexisting states; for example, the method of attractor annihilation by periodic modulation [21] can destabilize only those attractors whose eigenfrequencies are close to the modulation frequency [31]. In this paper, we address the question: Is it possible to design a method capable to eliminate all coexisting orbits except the one with desired properties, i.e. to make the system monostable at an orbit with dominant frequency of any one of the coexisting attractors? Our results give the positive answer to this question. In the following we will show how to design such a method, apply it to both non-autonomous and autonomous systems and test it experimentally in a multi-stable fiber laser with four coexisting periodic orbits.

Let us consider a general nonlinear dynamical system

$$\dot{\mathbf{x}}(t) = \mathbf{f}(\mathbf{x}(t), p), \qquad \mathbf{x} \in \mathbb{R}^n, \tag{1}$$

where $\mathbf{x} = (x_1, ..., x_j, ..., x_n)$ is the state vector and p is a parameter. We suppose that the system (1) exhibits the coexistence of q periodic or chaotic attractors $A = A_1, ..., A_q \subset \mathbb{R}^n$. Starting from a certain initial condition $\mathbf{x}(0) \in \mathbb{R}^n$, left to its own devices the system will reach a stable orbit A_i. We will show that both periodic modulation $u_c(t)$ and positive feedback kx_j (where $k > 0$ is the feedback strength) simultaneously applied to the system parameter as

$$p = p_0 + u_c(t) + kx_j \tag{2}$$

are able to transform the multistable system to a monostable one at orbit A_i^* with the same dominant frequency f_i as any preselected state A_i. In Eq. (2), p_0 is the parameter value prior

to the control, $u_c(t) = m_c \sin(2\pi f_c t)$ is the additional harmonic modulation with amplitude m_c and frequency f_c close to f_i of the selected orbit A_i being either periodic or chaotic. We will show how the combination of the external modulation and the positive feedback converts a multi-stable system with coexisting either periodic or chaotic orbits with pronounced dominant frequencies into a monostable system. Note, that our control method is invasive and cannot be applied to systems with coexisting steady state attractors.

Intuitively the physical mechanism underlying our method can be understood as follows. In a non-autonomous forced system, the coexisting stable periodic orbits are induced by the driving modulation and their frequencies are exactly subharmonics of the driving frequency. Evidently, the external modulation $u_c(t)$ at one of these subharmonic frequencies $f_c = f_i$ gets in resonance with this subharmonic frequency f_i. Due to the resonant interaction, the external forcing improves stability of the orbit A_i^* induced by the control modulation. Simultaneously, the feedback, depending on the sign of k, introduces a parabolic potential on the top of the system's phase space structure to favor A_i^*. Depending on how the parameter enters, a different potential might be created, so that the orbit A_i^* remains unique. Since it is not possible to get analytical solutions, the above speculations remain the hypothesis only based on our numerical simulations.

Although the final attractor A_i^* in the presence of the control Eq. (2) is not exactly the same as the original orbit A_i, both attractors possess the same dominant frequency in their power spectra and have a similar waveform; even though the outcome has a larger size. It should be noted that in a driven system, feedback alone cannot annihilate the orbit induced by the driving force (i.e. the period 1), but together with additional modulation it makes it happen. Unlike the Kapitza pendulum [32] and methods for dynamic stabilization of unstable states by parameter modulation [33–36], in our method we deal with already stable orbits, and the control aim is to destabilize undesired orbits and leave a single orbit.

The rest of the paper is organized as follows. First, in Sec. 2 we apply our method to a non-autonomous system, namely, to a fiber laser model with coexisting periodic orbits, test the method experimentally and compare experimental results with numerical simulations. Then, in Sec. 3 we extend our method to an autonomous system modeled by a Rössler-like oscillator with two coexisting chaotic attractors. Finally, main conclusions are given in Sec. 4.

NON-AUTONOMOUS SYSTEM

Multistable fiber laser with coexisting periodic orbits

In order to demonstrate how our method works in a real multistable system, we apply our approach to a diode-pumped erbium-doped fiber laser (EDFL) as an archetypical system with coexisting periodic orbits. The dynamics of the EDFL is described by the following rate equations [37, 38]

$$\frac{dP}{dt} = \frac{2L}{T_r} P \left\{ r_w \alpha_0 \left[N \left(\xi_1 - \xi_2 \right) - 1 \right] - \alpha_{th} \right\} + P_{sp}, \quad (3)$$
$$\frac{dN}{dt} = -\frac{\sigma_{12} r_w P}{\pi r_0^2} (N\xi_1 - 1) - \frac{N}{\tau} + P_{pump},$$

where P is the intracavity laser power, $N = \frac{1}{n_0 L} \int_0^L N_2(z) dz$ is the averaged (over the active fiber length L) population of the upper lasing level, N_2 is the upper level population at the z coordinate, n_0 is the refractive index of a "cold" erbium-doped fiber core, ξ_1 and ξ_2 are parameters defined by the relationship between cross sections of ground state absorption (σ_{12}), return stimulated transition (σ_{21}), and exited state absorption (σ_{23}). T_r is the photon intracavity round-trip time, α_0 is the small-signal absorption of the erbium fiber at the laser wavelength, α_{th} accounts for the intracavity losses on the threshold, τ is the lifetime of erbium ions in the excited state, r_0 is the fiber core radius, w_0 is the radius of the fundamental fiber mode, and r_w is the factor that conveys the match between the laser fundamental mode and erbium-doped core volumes inside the active fiber. The spontaneous emission into the fundamental laser mode is derived as

$$P_{sp} = N \frac{10^{-3}}{\tau T_r} \left(\frac{\lambda_g}{w_0} \right)^2 \frac{r_0^2 \alpha_0 L}{4\pi^2 \sigma_{12}}, \quad (4)$$

where λ_g is the laser wavelength. The pump power is expressed as

$$P_{pump} = P_p \frac{1 - \exp\left[-\alpha_0 \beta L \left(1 - N \right) \right]}{N_0 \pi r_0^2 L}, \quad (5)$$

where P_p is the pump power at the fiber entrance and β is a dimensionless coefficient. We explore the following parameter values: $L = 0.88$ m, $T_r = 8.7$ ns, $r_w = 0.308$, $\alpha_0 = 40$ m^{-1}, $\xi_1 = 2$, $\xi_2 = 0.4$, $\alpha_{th} = 3.92 \times 10^{-2}$, $\sigma_{12} = 2.3 \times 10^{-17}$ m^2, $r_0 = 2.7 \times 10^{-6}$ m, $\tau = 10^{-2}$ s, $\lambda_g = 1.65 \times 10^{-6}$ m, $w_0 = 3.5 \times 10^{-6}$ m, $\beta = 0.5$, and $N_0 = 5.4 \times 10^{25}$ m^{-3}, that correspond to the real experimental conditions which will be described in the following section.

Under harmonic modulation $m_d \sin(2\pi f_d t)$ within a certain range of driving amplitude m_d and frequency f_d the laser exhibits the coexistence of four periodic orbits A_i ($i = 1, 3, 4, 5$) at the driving frequency and its subharmonics $f_i = f_d / i$ [37]. To select a particular orbit we apply both an additional harmonic modulation $m_c \sin(2\pi f_c t)$ and a positive feedback kP to the diode pump current, so that the pump parameter becomes

$$P_p = p_0 \left[1 - m_d \sin(2\pi f_d t) + m_c \sin(2\pi f_c t) + kP \right]. \quad (6)$$

In Fig. 1 we demonstrate a glimpse of the results with the time series, which illustrate the efficiency of our method in making the laser monostable at any of possible periodic orbits. No matter from which initial state we started, the control

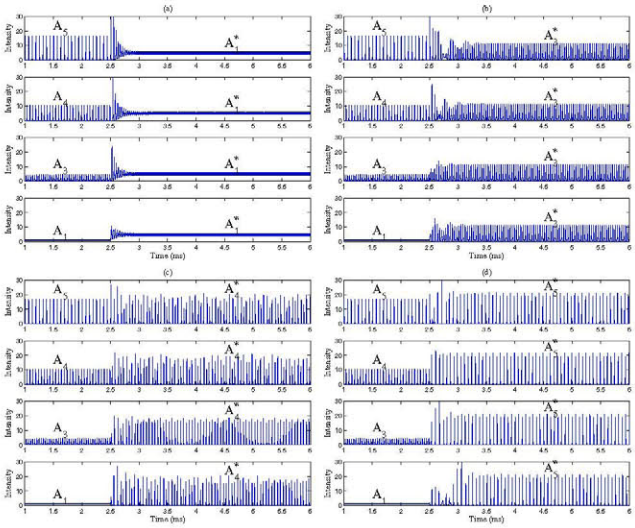

FIG. 1. Time series demonstrating transitions from every attractor to a monostable state of period (a) $i = 1$, (b) $i = 3$, (c) $i = 4$, and (d) $i = 5$, under control with $k = 0.4$ and $f_c = f_i$. $f_d = 80$ kHz, $m_d = 1$.

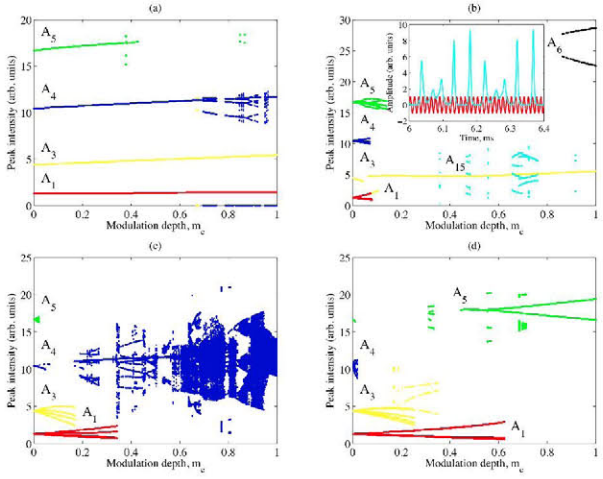

FIG. 2. Numerical bifurcation diagrams of laser peak intensity versus modulation depth when only additional harmonic modulation (without feedback) is applied with (a) $f_c = f_1$, (b) $f_c = f_3$, (c) $f_c = f_4$, and (d) $f_c = f_5$. $k = 0$, $m_d = 1$, $f_d = 80$ kHz. The initial conditions are randomly varied. The inset in (b) shows the time series for the period-15 attractor.

destabilizes all attractors except one A_i^* with dominant frequency f_i of the preselected orbit A_i, thus making the laser monostable.

To reveal mechanisms underlying our method, we consider separately the effects of the harmonic modulation and the positive feedback. Figure 2 shows the bifurcation diagrams of the laser peak intensity for every coexisting attractor when only harmonic modulation with frequency $f_c = f_i$ is applied. Although the peak amplitude varies from pulse to pulse, the phase is locked by the control, so that the attractors are enclosed within a torus hull. Since the repetition rate of the laser pulses is independent of the modulation depth, the attractor periodicity is easily defined via sections through the torus.

One can see that without feedback ($k = 0$) even 100% modulation ($m_c = 1$) is not capable of making the laser monostable at an orbit with dominant frequency of any orbit prior to the control. Some subharmonic orbits with frequencies differed from f_i are destroyed, while other attractors arise. For instance, when $f_c = f_3$ [Fig. 2(b)] the period-1, 4, and 5 attractor branches disappear at $m_c \approx 0.1$, while new orbits appear. Interestingly, we detect stable periodic orbits with higher periods which did not exist without control, e.g. the period-6 (A_6) and period-15 (A_{15}). The time series of the period-15 attractor are shown in the inset of Fig. 2(b). As m_c is increased, some states can undergo period-doubling bifurcations and even become chaotic, as, for example, the branches starting from the period-4 orbit in Fig. 2(c) and from the period-5 orbit in Fig. 2(d).

On the other hand, the feedback alone ($m_c = 0$) allows monostability for the period-1 attractor only. As seen from the bifurcation diagram in Fig. 3, the increasing feedback strength consequently destabilizes period-5, 4, and 3 orbits, so that the single period-1 (A_1^*) attractor remains. Even though we can reach a monostable system, neither modulation nor feedback by itself gives the selection option to the researcher.

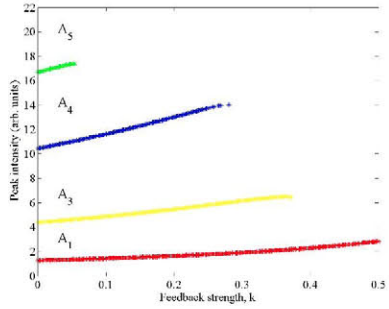

FIG. 3. Numerical bifurcation diagrams of laser peak intensity versus feedback strength when no additional external modulation is applied. $m_c = 0$, $m_d = 1$, $f_d = 80$ kHz. The initial conditions are randomly varied.

The numerical state diagrams in Fig. 4 illustrate the combined effect of the harmonic modulation and the positive feedback. Each diagram represents the green region where only one attractor exists. Note, that in other (blue) regions monostability is also possible, but for other attractors. For example, without control modulation ($m_c = 0$) or for very small m_c, a single period-1 attractor is observed for $k > 0.4$.

To demonstrate that the blue pixels inside of the green regions in Fig. 4 do correspond to multistable regimes, we calculate the bifurcation diagrams for $f_c = f_3$ using m_c as a control parameter for three different feedback strengths ($k = 0.1, 0.25, 0.5$) and randomly varying initial conditions. From these diagrams in Fig. 5 one can see that the system is monostable at the period-3 orbit within a certain range of m_c and the region of monostability enlarges as m_c increases,

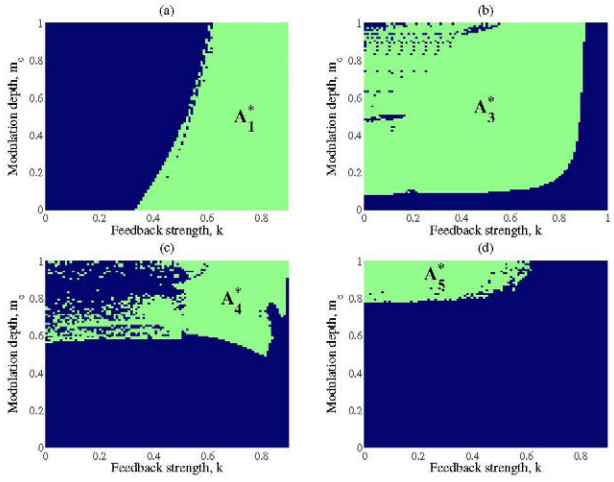

FIG. 4. Numerical state diagrams in (k, m_c)-parameter space when control modulation at frequency (a) f_1, (b) f_3, (c) f_4, and (d) f_5 is applied. Monostability is found in the light regions.

while the peak intensity becomes higher. The alternation of multi-stable and monostable regimes, as m_c is varied, is evidently seen in the basins of attraction of the coexisting states shown in Fig. 6. One can see that the system is monostable at the A_3^* attractor for $k = 0.1$ and $m_c = 0.12$ [Fig. 6(b)]. The comparison of the bifurcation diagrams in Fig. 5 and the basins of attraction in Fig. 6 with the state diagrams in Fig. 4(b) justifies that the appearance of the blue pixels inside the green regions in Fig. 4 is not a numerical artifact.

The efficiency of our method in controlling the number of coexisting attractors is demonstrated in Fig. 7, where we plot the basins of attraction of the periodic orbits when $f_c = f_5$. While for very small control amplitude $m_c = 0.0065$ without feedback ($k = 0$) four attractors coexist [Fig. 7(a)], for larger amplitude $m_c = 0.168$ and with feedback $k = 0.5$ three attractors coexist [Fig. 7(b)]. For the same feedback and $m = 0.79$ two attractors coexist [Fig. 7(c)], and finally for $m = 0.9$ only one period-5 attractor (A_5^*) remains [Fig. 7(d)]. With the same dominant frequency and a similar waveform, it is clear that the basin of attraction of A_5^* is much larger than the basin of attraction of the original attractor A_5, which for most applications is an asset. Note that the changes in m_c in the four panels of Fig. 7 are not small. From (a) to (b) m_c increases 25 times, from (b) to (c) almost 5 times, and from (c) to (d) almost 2 times.

Monostability at A_i^* can also be achieved if the control frequency f_c is tuned a little with respect to the dominant frequency f_i of a desired orbit A_i. However, the efficiency in this case is much lower, i.e. a stronger control (higher amplitude m_c) is required. The sensitivity of the system to the frequency mismatch $\Delta = f_i - f_c$ is different for different attractors. When the detuning Δ is too large, the method does not work. A similar situation occurs for an autonomous chaotic system which dominant frequency is determined by its natural frequency.

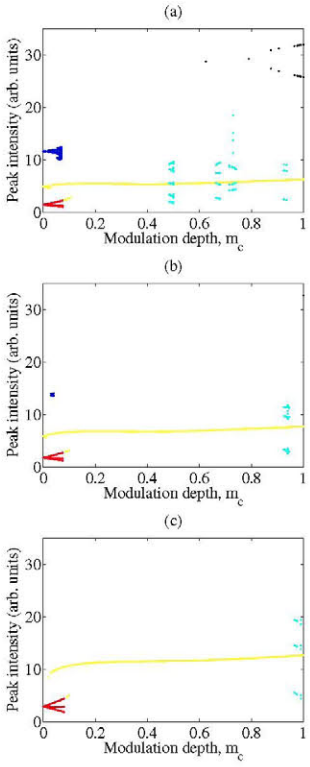

FIG. 5. Numerical bifurcation diagrams for $f_c = f_3$ with m_c as a control parameter at (a) $k = 0.1$, (b) 0.25, and (c) 0.5, calculated for thirty randomly varied initial conditions. The monostable and multi-stable regions alternate as m_c is varied.

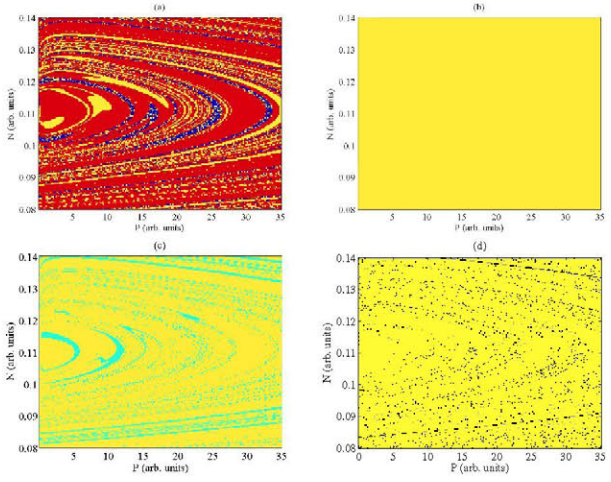

FIG. 6. Basins of attraction of period-1, period-3, period-4, period-6, and period-15 orbits for $f_c = f_3$ at $k = 0.1$ and (a) $m_c = 0.07$, (b) 0.12, (c) 0.49, and (d) 0.97.

Experimental evidence

The experimental setup is shown in Fig. 8. The EDFL contains the erbium-doped fiber (EDF) and two fiber Bragg gratings (FBG1 and FBG2). The EDFL is pumped by a laser diode (LD) through the polarization controller (PC) and the

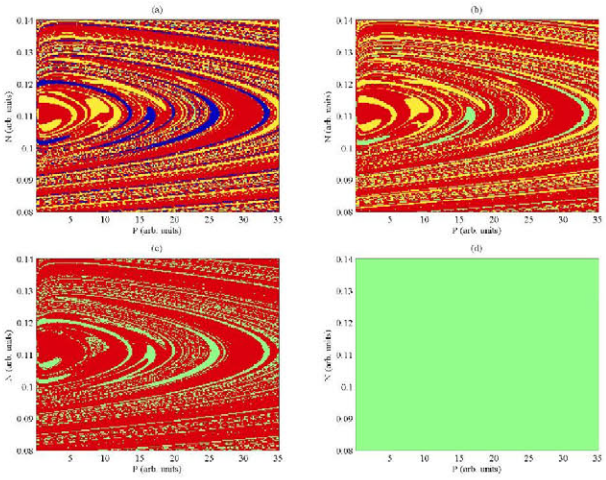

FIG. 7. Basins of attraction of coexisting periodic orbits in the laser with control modulation at $f_c = f_5$ for (a) $m_c = 0.0065$, $k = 0$, (b) $m_c = 0.168$, $k = 0.5$, (c) $m_c = 0.79$, $k = 0.5$, and (d) $m_c = 0.9$, $k = 0.5$.

wave-division multiplexer (WDM). The EDFL output is detected by a photodetector (PD) and analyzed with an oscilloscope (OSC). The optical isolator (OI) in front of the detector avoids an optical feedback from the detector window to the EDFL. The signal recorded by the photodetector and amplified enters to the diode current controller (DCC) of the diode pump laser. The waveform generators WFG1 and WFG2 produce periodic signals for driving and control respectively, to be also sent to the DCC.

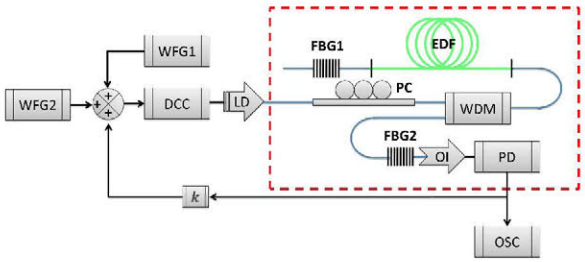

FIG. 8. Experimental setup of the diode-pumped erbuim-doped fiber laser with monostability control. EDF is the erbium-doped fiber, FBG1 and FBG2 are the fiber Bragg gratings, LD is the pump laser diode, DCC is the diode current controller, PC is the polarization controller, WDM is the wave-division multiplexer, OI is the optical isolator, PD is the photodetector, OSC is the oscilloscope, WFG1 and WFG2 are the waveform generators, and K is the coupling interface.

The oscilloscope traces in Fig. 9 illustrate the experimental realization of the monostability control in the EDFL. First, we apply the positive feedback and then harmonic modulation with frequency $f_c = f_d/i$ $(i = 3, 4, 5, 6)$. The control annihilates all attractors and leaves only A_i^*, thus converting the multi-stable laser to monostable. Interestingly, in the experiment we are able to stabilize orbit A_6^*, whereas orbit A_6 is unstable without the control.

Figures 10 shows the experimental state diagrams for the

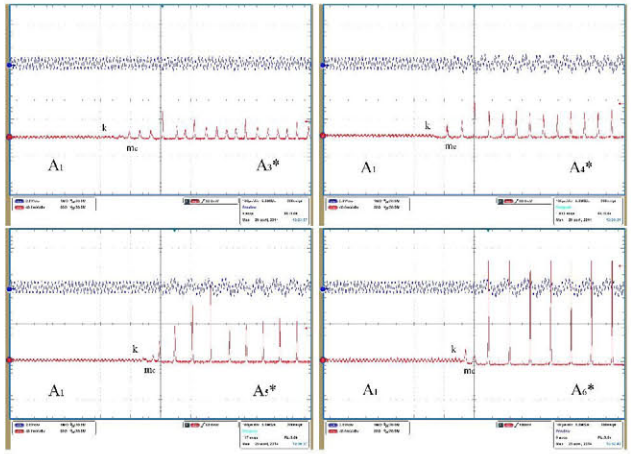

FIG. 9. Oscilloscope traces demonstrating transitions from original period-1 to new (a) period-3, (b) period-4, (c) period-5, and (d) period-6 attractors after application of positive feedback with $k = 0.4, 0.8, 0.4, 0.4$ at 400 μs and harmonic modulation with $f_c = f_i$ $(i = 3, 4, 5, 6)$ and $m_c = 0.3, 0.6, 0.6, 0.6$ (180, 360, 360, 360 mVpp) at 480 μs. The upper trace is the signal applied to the diode pump current and the lower trace is the laser response. $f_d = 80$ kHz.

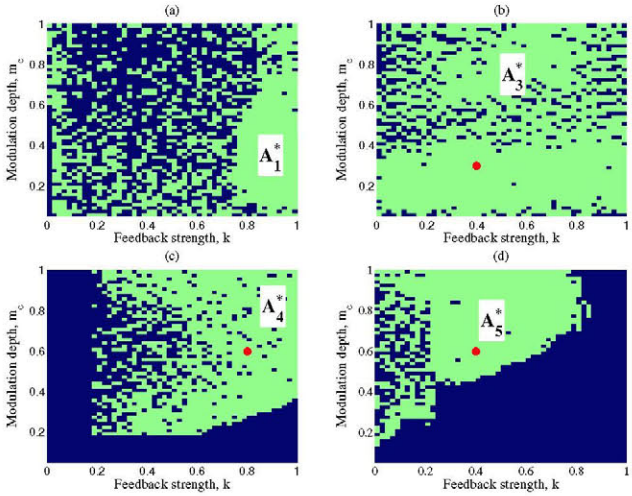

FIG. 10. Experimental state diagrams in (k, m_c)-parameter space for (a) $f_c = f_1$, (b) $f_c = f_3$, (c) $f_c = f_4$, and (d) $f_c = f_5$. Monostability with attractor A_i^* is found in the light and multistability in the dark regions. The dark dots in (b-d) indicate the parameters for the time series in Figs. 9(a-c).

period-1, period-3, period-4, and period-5 attractors in space of the modulation depth and feedback strength when the control modulation with $f_c = f_i$ is applied. Although the numerical and experimental results are in a good qualitative agreement, the range of experimental parameters for monostability is larger than that of numerical ones. This means that the method works better in practice than in theory. This occurs because small noise, inevitable in experiments, helps in the attractor selection, i.e. in the presence of noise the system switches to the desired attractor easier than without noise. The

final attractor is globally stable and robust to noise because the system is monostable.

AUTONOMOUS SYSTEM

In order to check the validity of our approach for autonomous systems, we apply our method to a piecewise Rössler oscillator with two coexisting chaotic attractors [39] characterized by distinct dominant frequencies (f_{C_1} and f_{C_2}) in their power spectra shown in Fig. 11(a). This oscillator is modeled as [40]

$$\frac{dx}{dt} = -\alpha_1 \left(x + \beta y + \Gamma z\right), \tag{7}$$

$$\frac{dy}{dt} = -\alpha_2 \left(-\gamma x - \delta y\right), \tag{8}$$

$$\frac{dz}{dt} = -\alpha_3 \left(-f(x) + z\right), \tag{9}$$

$$f(x) = \begin{cases} 0 & x \leq 3 \\ \mu\,(x-3) & x > 3, \end{cases} \tag{10}$$

with parameters $\alpha_1 = 500$, $\alpha_2 = 200$, $\alpha_3 = 10000$, $\Gamma = 20$, $\gamma = 50$, $\delta = 14.625$, and $\mu = 15$. The system with $\beta = 10$ exhibits the coexistence of two chaotic attractors C_1 and C_2 (Figs. 11(b)). In the following we will show that the control applied to the parameter β as $\beta = 10 + m_c \sin(2\pi f_c t) + ky$ makes the system monostable at the attractor similar to one of the preselected states.

Figure 11 shows the power spectra and phase-space trajectories of the two coexisting chaotic attractors C_1 and C_2 in the original bistable Rössler-like oscillator (Fig. 11(a,b)). New chaotic attractors C_1^* and C_2^* in the monostable system have the same dominant frequencies as the original attractors and similar complexity. The difference in the attractor size appears due to different sizes of the basins of attraction of the original states. The destruction of C_1 requires much stronger external intervention since its basin of attraction is much larger than the basin of C_2.

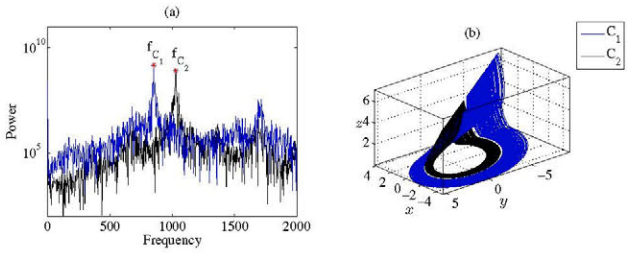

FIG. 11. (a) Power spectra and (b) phase-space portraits of bistable Rössler-like oscillator. The coexisting C_1 and C_2 chaotic attractors are shown, respectively, by the grey and black curves.

The efficiency of the method for making the system monostable can be seen from the basins of attraction shown in Fig. 12. One can see that the basin of attraction of every final monostable state is the phase space occupied by the two original attractors.

In addition to their dominant frequencies in the power spectra, the chaotic attractors are distinguished by their complexity. The system complexity can be quantitatively characterized by the normalized permutation entropy given as [41]

$$H[P] = S[P]/S_{max}, \tag{11}$$

where $S[P] = -\sum_{i=1}^{N} p_i \log p_i$ and $S_{max} = \log N$ with $N = D!$ being the total number of vectors over which the probability distribution P is computed, and D is the embedding dimension.

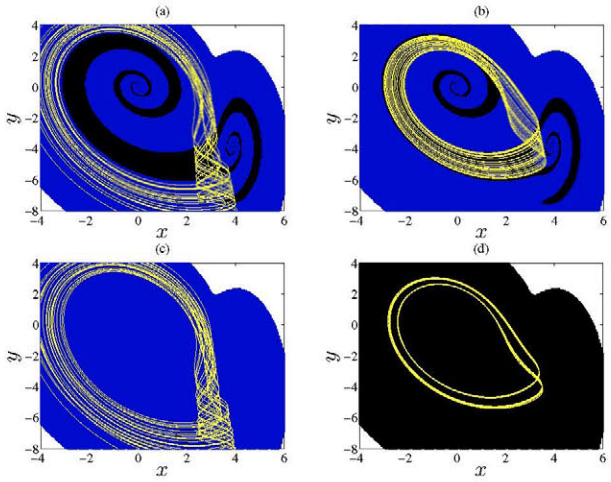

FIG. 12. Basins of attraction of chaotic attractors C_1 (grey area), C_2 (black area), and infinity attractor (white area) in (a,b) original bistable Rössler-like oscillator and (c,d) final monostable system under control with (c) $f_c = f_{C_1}$, $m_c = 0.5$, $k = 0.05$ and (d) $f_c = f_{C_2}$, $m_c = 0.725$, $k = 0.025$. The light curves show (a,b) the original and (c,d) final attractors.

Using the algorithm described in [42, 43], we calculate the system complexity when the control is applied. The results are shown in Fig. 13, where the colors indicate the normalized permutation entropy calculated by Eq. (11) in the parameter space of the feedback strength and modulation depth for two different modulation frequencies, f_{C_1} [Fig. 13(a)] and f_{C_2} [Fig. 13(b)]. These diagrams are calculated using random initial conditions. One can see that the complexity of the final attractor of the controlled monostable system is only a little lower than that of the corresponding original attractor, while the difference between the perturbation entropies of the two coexisting states are pronounced. This indicates that although our control method is invasive, the attractors in the bistable and monostable systems are very similar.

Monostability can also be distinguished by other measures, for example, by the dominant frequency in the power spectrum or the global maximum of the z-component, as seen from Fig. 11. However, only complexity indicates how much the final attractor differs from the original one. Since our system is deterministic, the random patterns in Fig. 13 correspond to having either C_1^* or C_2^* depending on the initial conditions, that means bistability. Instead, the homogeneous color zones

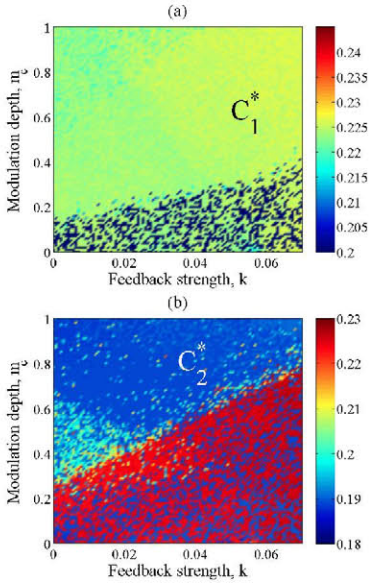

FIG. 13. Normalized permutation entropy Eq. 11 of the Rössler-like oscillator as a function of k and m_c for (a) $f_c = f_{C_1}$ and (b) $f_c = f_{C_2}$. The homogeneous areas in the upper part of the diagrams indicate the regions of the same or similar complexity meaning monostability at the C_1^* and C_2^* attractors.

in the upper parts of the diagrams mean that the system complexity is almost independent of the control parameters and initial conditions, i.e. only one attractor exists.

CONCLUSION

We have shown that a multi-stable system can be converted into a monostable one by simply applying an external harmonic modulation and a positive feedback to a system parameter. The efficiency of the proposed method has been demonstrated in both non-autonomous and autonomous systems with coexisting either periodic or chaotic attractors with distinct dominant frequencies in their power spectra.

One of the main advantages of our method is its easy implementation for practical applications. Even without preliminary knowledge of the system dynamics, one can select attractors by organizing a positive feedback and tuning the generator frequency. The method can be prominent for technological applications where giant pulses are required. It may also find important applications in medicine, e.g. for designing a pacemaker enable to stabilize the cardiac rhythm at a desired frequency.

[1] Arecchi FT, Meucci R, Puccioni GP, Tredicce J. 1982 Experimental evidence of subharmonic bifurcations, multistability, and turbulence in a Q-switched gas laser. *Phys. Rev. Lett.* **49**, 1217–1220.

[2] Pisarchik AN, Barmenkov YO, Kir'yanov AV. 2003 Experimental demonstration of attractor annihilation in a multistable fiber laser. *Phys. Rev. E* **68**, 066211.

[3] Ngonghala CN, Feudel U, Showalter K. 2011 Extreme multistability in a chemical model system. *Phys. Rev. E* **83**, 056206.

[4] Pisarchik AN, Feudel U. 2014 Control of multistability. *Phys. Rep.* **540**, 167–218.

[5] Robinson A, Calov R, Ganopolski, A. 2012 Multistability and critical thresholds of the Greenland ice sheet. *Nature Clim. Change* **2**, 429–432.

[6] Wolf F. 2005 Symmetry, multistability, and long-range interactions in brain development. *Phys. Rev. Lett.* **95**, 208701.

[7] Kelso, A. S. 2012 Multistability and metastability: understanding dynamic coordination in the brain. *Phil. Trans. R. Soc. B* **367**, 906–918.

[8] Mincheva M, Craciun G. 2008 Multigraph conditions for multistability. *Proc. IEEE* **96**, 1281–1291.

[9] Malashchenko T, Shilnikov A, Cymbalyuk G. 2011 Six types of multistability in a neuronal model based on slow calcium current. *PlosOne* **6**, e21782.

[10] Marco MD, Forti M, Grazzini M, Pancioni L. 2014 Necessary and sufficient condition for multistability of neural networks evolving on a closed hypercube. *Neural Networks* **54**, 38–48.

[11] Cohen MA, Grossberg S. 1983 Absolute stability of global pattern formation and parallel memory storage by competitive neural networks. *IEEE Trans. on Systems, Man, and Cybernetics* **13**, 815–826.

[12] Hopfield JJ. 1984 Neurons with graded response have collective properties like those of two-state neurons. *Proc. Nat. Acad. Sci.* **81**, 3088–3092.

[13] Wang L. 2013 Dynamical analysis on the multistability of high-order neural networks. *Neurocomputing* **110**, 137–144.

[14] Ikeda K, Matsumoto K. 1987 High dimensional chaotic behavior in systems with time delayed feedback. *Physica D* **29**, 223–235.

[15] Martínez-Zérega BE, Pisarchik AN, Tsimring LS. 2003 Using periodic modulation to control coexisting attractors induced by delayed feedback. *Phys. Lett. A* **318**, 102–111.

[16] Pyragas K 1992 Continuous control of chaos by self-controlling feedback. *Phys. Lett. A* **170**, 421–428.

[17] Poon L, Grebogi, C. 1995 Controlling complexity. *Phys. Rev. Lett.* **75**, 4023–4026.

[18] Feudel U, Grebogi C. 1997 Multistability and control of complexity. *Chaos* **7**, 597–604.

[19] Geltrude A, Meucci R, Arecchi FT. 2012 Feedback control of bursting and multistability in chaotic systems. *Commun. Nonlinear Sci. Numer. Simulat.* **17**, 3031–3039.

[20] Cornelius SP, Kath WL, Motter AE. 2013 Realistic control of network dynamics. *Nat. Commun.* **4**, 1942.

[21] Pisarchik AN, Goswami BK. 2000 Annihilation of one of the coexisting attractors in a bistable system. *Phys. Rev. Lett.* **84**, 1423–1426.

[22] Pisarchik AN. 2001 Controlling the multistability of nonlinear systems with coexisting attractors. *Phys. Rev. E* **64**, 046203.

[23] Pisarchik AN, Barmenkov YO, Kir'yanov AV. 2003 Experimental characterization of the bifurcation structure in an erbium-doped fiber laser with pump modulation. *IEEE J. Quantum. Electron.* **39**, 1567–1571.

[24] Banerjee S. 1997 Coexisting attractors, chaotic saddles and fractal basins in a power electronic circuit. *IEEE Trans. Circuits Syst. I* **44**, 847–849.

[25] Dhamala M, Lai YC. 1999 Controlling transient chaos in deterministic flows with applications to electrical power systems and ecology. *Phys. Rev. E* **59**, 1646–1655.

[26] Li C, Sprott JC. 2013 Multistability in a butterfly flow. *Int. J. Bifur. Chaos* **2**3, 1350199.
[27] Baer T. 1986 Large-amplitude fluctuations due to longitudinal mode coupling in diode-pumped intracavity-doubled Nd:YAG lasers. *J. Opt. Soc. Amer. B* **3**, 1175–1179.
[28] Walleczek J, Editor. 2000 *Dynamics and Nonlinear Control*, Cambridge: University Press.
[29] Glass L. 2005 Multistable spatiotemporal patterns of cardiac activity. *Proc. Natl. Acad. Sci. USA* **1**02, 10409–10410.
[30] Surovyatkina E, Noble D, Gavaghan D, Sher A. 2010 Multistability property in cardiac ionic models of mammalian and human ventricular cells. *Prog. Biophys. Mol. Biol.* **1**03, 131–141.
[31] Goswami BK, Pisarchik AN. 2008 Controlling multistability by small periodic perturbation. *Int. J. Bifur. Chaos* **1**8 1645–1673.
[32] Kapitza PL. 1951 Dynamic stability of a pendulum when its point of suspension vibrates. *Sov. Phys. JETP* **2**1 588–592.
[33] Mandel P, Erneux T. 1984 Laser Lorenz equations with a time-dependent parameter. *Phys. Rev. Lett.* **5**3 1818–1820.
[34] Pisarchik AN, Chizhevsky VN, Corbalán R, Vilaseca R. 1997 Experimental control of nonlinear dynamics by slow parametric modulation. *Phys. Rev. E* **5**5 2455–2461.
[35] Pisarchik AN. 1998 Dynamical tracking unstable periodic orbits. *Phys. Lett. A* **2**42 152–162.
[36] Pisarchik AN, Corbalán R, Chizhevsky VN, Vilaseca R, Kuntsevich BF. 1998 Dynamic stabilization of unstable periodic orbits in a CO_2 laser by slow modulation of cavity detuning. *Int. J. Bifurcat. and Chaos* **8** 1783–1789.
[37] Pisarchik AN, Kir'yanov AV, Barmenkov YO, Jaimes-Reátegui R. 2005 Dynamics of an erbium-doped fiber laser with pump modulation: theory and experiment. *J. Opt. Soc. Am. B* **2**2, 2107–2114.
[38] Pisarchik AN, Jaimes-Reátegui R, Sevilla-Escoboza R, Huerta-Cuellar G, Taki, M. 2011 Rogue waves in a multistable fiber laser. *Phys. Rev. Lett.* **1**07, 274101.
[39] Pisarchik AN, Jaimes-Reátegui R, Villalobos-Salazar JR, Garcia-Lopez JH, Boccaletti S. 2006 Synchronization of chaotic systems with coexisting attractors. *Phys. Rev. Lett.* **9**6, 244102.
[40] Pisarchik AN, Jaimes-Reátegui R, Garcia-Lopez JH. 2008 Synchronization of coupled bistable chaotic systems: Experimental study. *Phil. Trans. R. Soc. A* **3**66, 459–473.
[41] Bandt C, Pompe B. 2002 Permutation entropy: a natural complexity measure for time series. *Phys. Rev. Lett.* **8**8, 174102.
[42] López-Ruiz R, Mancini HL, Calbet X. 1995 A statistical measure of complexity. *Phys. Lett. A* **2**09, 321–326.
[43] Calbet X, López-Ruiz R. 2001 Tendency toward maximum complexity in a non-equilibrium isolated system. *Phys. Rev. E* **6**3, 066116.